

Friction phenomena and phase transition in the underdamped two-dimensional Frenkel-Kontorova model

Yang Yang,¹ Wen-Shan Duan,^{1,*} Jian-Min Chen,² Lei Yang,³ Jasmina Tekić,⁴ Zhi-Gang Shao,⁵ and Cang-Long Wang¹

¹Department of Physics, Northwest Normal University, Lanzhou 730070, People's Republic of China

²State Key Laboratory of Solid Lubrication, Lanzhou Institute of Chemical Physics, Chinese Academy of Science, Lanzhou 730000, People's Republic of China

³Institute of Modern Physics, Chinese Academy of Science, Lanzhou, People's Republic of China and Department of Physics, Lanzhou University, Lanzhou 730000, People's Republic of China

⁴Theoretical Physics Department 020, "Vinča" Institute of Nuclear Sciences, P. O. Box 522, 11001 Belgrade, Serbia

⁵Laboratory of Quantum Information Technology, Institute of Condensed Matter Physics, School of Physics and Telecommunication Engineering, South China Normal University, 510006 Guangzhou, People's Republic of China

(Received 9 February 2010; revised manuscript received 17 May 2010; published 16 November 2010)

Locked-to-sliding phase transition has been studied in the driven two-dimensional Frenkel-Kontorova model with the square symmetric substrate potential. It is found that as the driving force increases, the system transfers from the locked state to the sliding state where the motion of particles is in the direction different from that of driving force. With the further increase in driving force, at some critical value, the particles start to move in the direction of driving force. These two critical forces, the static friction or depinning force, and the kinetic friction force for which particles move in the direction of driving force have been analyzed for different system parameters. Different scenarios of phase transitions have been examined and dynamical phases are classified. In the case of zero misfit angle, the analytical expressions for static and kinetic friction force have been obtained.

DOI: [10.1103/PhysRevE.82.051119](https://doi.org/10.1103/PhysRevE.82.051119)

PACS number(s): 64.60.-i, 68.35.Af, 05.45.Yv, 81.40.Pq

I. INTRODUCTION

A chain of interacting particles subjected to an either random or periodic substrate potential represents one of the most tractable models for studying the nonequilibrium behavior and dynamical phase transitions in a wide variety of condensed matter systems such as vortex lattices in superconductors [1,2], Josephson junction, charge-density waves [3], colloids [4], Wigner crystals [5], metallic dots [6,7], magnetic bubble arrays [8], and systems in tribology [9,10]. In both theoretical and experimental studies of these systems, the attention has been always focused on the behavior, motion, dynamical phases, and the structure of the lattice when the external driving force is varied. The results have shown that the system parameters such as winding number, external driving force, pinning, interaction between atoms, damping, and geometry of the substrate play the crucial role in the scenarios of the transition phenomena and properties of dynamical phases.

Due to significance for the studies of vortex dynamics in superconductors, the overdamped motion of an array of interacting particles over a random substrate potentials has been studied extensively during past several years. In an array of vortices, dynamical phases have been classified and their dependence on the elastic constant and the external driving force has been examined [11–13]. The phase transition from the locked state to an ordered sliding state has been observed experimentally in superconducting flux lattices [14–17].

The locked-to-sliding phase transition in the overdamped driven two-dimensional Frenkel-Kontorova (2DFK) model

with different symmetries (square or triangular) of the periodic substrate potential has been studied by Reichhardt *et al.* for the system of vortices in superconductors [18–21]. The system behavior depends on the dimensionless concentration, which is defined as the ratio between the number of atoms and the number of minima of the substrate potential. In the commensurate case, the critical depinning force is larger than in the incommensurate case, and transition from an ordered locked phase to the sliding state that corresponds to the moving crystal or the “elastic flow phase” appears [19].

Direction of the external driving force may also strongly influence the behavior of system. In an overdamped system with repulsively interacting atoms on the triangular substrate, when direction of driving force was varied, an interesting phenomenon has been observed [22]. The atomic flow was not in the direction that was aligned with the external driving force, but in one of the symmetry axes of the substrate.

Contrary to the numerous studies of the overdamped FK model, a relatively small number of studies have been dedicated to driven underdamped 2DFK model [one-dimensional (1D) underdamped FK model has been extensively studied due to its applications in different branches of science] [23–31]. Several authors have previously studied the 2D elastic lattice under periodic substrate potential and the random impurity potential by using the 2DFK model [32–36]. Tekić *et al.* studied the locked-to-sliding transition in the underdamped isotropic 2DFK model with the triangular substrate potential [36]. They have found that when the driving force increases, the system transfers from a disorder locked state to an ordered sliding state that corresponds to a moving crystal. Depending on the system parameters, during this transition, different scenarios and intermediate phases may appear.

*duanws@nwnu.edu.cn

Recently, in the experimental studies in nanotribology, in the measuring of the friction force between two contacting layers, strong influence of the misfit angle on the friction force has been observed. According to results, superlubricity (the state of vanishing friction) may appear for certain values of misfit angle [37,38]. In such contact, the ratio between the lattice units of the surfaces must be irrational along the sliding direction so that each individual atom receives different amount of force from different directions. These forces consequently offset each other resulting in superlubricity. This offsetting of forces appears due to the continuous motion of atoms that may be the basic principle of the superlubricity. These results are in great analogy with the results found in superconductivity [19–22] what motivates further theoretical studies since an understanding of the origin of the friction force at the microscopic level could represent a theoretical guidance for the designing of smart materials for both industrial and biomedical applications [39,40].

Motivated by the above-mentioned theoretical [36] and experimental [14,15] studies, in this paper, we will study the locked-to-sliding phase transition in 2DFK model. Our focus was on the examination of different scenarios and properties of dynamical phases as the system parameters change. It was found that as the driving force increases, the system transfers to the sliding state where the motion of particles is in the direction different from that of driving force. With the further increase in driving force, at some critical value, the particles start to move in the direction of driving force. Dynamical phases have been classified and the properties of critical forces at which these transitions appear have been studied in detail. These critical forces, the static friction force or the depinning one, and the kinetic friction force or the one for which particles start to move in the direction of driving force depend on the direction and the magnitude of external driving force, the magnitude of adhesive force, the interaction strength between two atoms in the upper layer and, in particular, on the misfit angle θ . For the case of zero misfit angle $\theta=0^\circ$, their analytical expressions have been obtained.

The paper is organized as follows. In Sec. II, the model is proposed. Numerical results and discussions are presented in Sec. III. Finally, Sec. IV, concludes the paper.

II. MODEL

We consider the two-dimensional lattice of particles with harmonic interaction (upper layer) coupled to a static pinning potential (lower layer). The upper layer has a square periodicity where the neighbors of each particle are fixed, and it is driven by an external driving force F_{ext} . The square symmetric substrate potential is given as follows [41,42]:

$$V_{\text{sub}}(x, y) = -\frac{f}{2\pi} \left[\cos\left(\frac{2\pi}{b}\sqrt{2}x\right) + \cos\left(\frac{2\pi}{b}\sqrt{2}y\right) \right]. \quad (1)$$

Equation (1) represents the first term of the Fourier series of 2D substrate potential with square periodicity such as the substrate surface of NaCl. In Refs. [41,42], its expression is given in the form: $V_{\text{NaCl}}(x, y) = -\frac{E_0}{2} \cos\left(\frac{2\pi}{b}x\right) \cos\left(\frac{2\pi}{b}y\right)$. However, by the coordinate transformation of $x+y=x'$, $x-y=y'$,

it becomes Eq. (1). The position vector $\mathbf{r}_{n,m}$ of an arbitrary (n, m) th atom satisfies the following equation of motion:

$$M_{n,m} \ddot{\mathbf{r}}_{n,m} + \gamma M_{n,m} \dot{\mathbf{r}}_{n,m} + \frac{\partial(V_{\text{int}} + V_{\text{sub}})}{\partial \mathbf{r}_{n,m}} = \mathbf{F}_{\text{ext}}, \quad (2)$$

where for the diatomic molecular system, $M_{n,m}=M_1$ is the mass of the atom if $n+m$ is an odd number and $M_{n,m}=M_2$ if $n+m$ is an even number. For the monatomic molecular system, we assume $M_1=M_2=1$. γ is damping coefficient where in our work the simulations have been performed for $\gamma=0.1$. Throughout the paper, we will use dimensionless variables, where $b/\sqrt{2}$ is the lattice constant, we take $b=1$, $\mathbf{F}_{\text{ext}} = (F_{\text{ext}} \cos \alpha, F_{\text{ext}} \sin \alpha)$ is the external driving force, and α is the angle between the directions of \mathbf{F}_{ext} and the unit vector of x axis. V_{int} is the interaction potential between particles of the upper layer that has the following harmonic form: $V_{\text{int}} = \frac{K}{2}[(r-l_0)^2]$ for small amplitude waves, with a strength K . Equilibrium distance is $l_0=a$ between the nearest neighbors and $l_0=\sqrt{2}a$ between the next nearest neighbors, where a is defined as $a=L_x/N=L_y/M$. L_x and L_y are the length in the x and y directions of the 2D system, N and M are the number of minima in the substrate potential in the x and y direction, respectively. a is the substrate periodicity, we take $a=1$ and only consider the interactions among the nearest and the next nearest neighbors.

Underdamped regime correspond to the situation when $\gamma^2 - 4\omega_0^2 < 0$, where $\omega_0 = \frac{2\sqrt{\pi}f}{\sqrt{Mb}}$ represents characteristic frequencies of the system. The range of f we choose in this paper is $0.1 < f < 1.5$, then the minimum value of characteristic frequency is about 1.1. The damping term we choose in this paper is $\gamma=0.1$ which is much smaller than the characteristic frequencies. Therefore, all the situations we study in this paper are in the underdamped regime.

In general, for the systems in which the orientations of the two layers do not match, we rotate the lower layer respect to x axis by an arbitrary misfit angle θ . Then $\begin{pmatrix} x' \\ y' \end{pmatrix} = \begin{pmatrix} \cos \theta & -\sin \theta \\ \sin \theta & \cos \theta \end{pmatrix} \begin{pmatrix} x \\ y \end{pmatrix}$. The periodic boundary condition is imposed for misfit angle θ to enforce a fixed density condition for the system. the density ρ is defined as particle numbers per periodicity of lower layers, namely, $\rho=b/a$. In this paper $\rho=1$. Meanwhile, the neighbors of each particle are independent of the misfit angle.

The numerical procedure used for solving the above equations was the same as in the previous works [23,35]. We considered the atomic layer of $N \times M = 12 \times 12$ atoms placed onto substrate. The velocity and position of each particle are in their equilibrium position before rotating the lower layer with respect to x axis by misfit angle. The boundary conditions do not create a defect. then the dc force was adiabatically increased from zero with the step $\Delta F=0.005$. Equation (2) has been integrated using the fourth-order Runge-Kutta algorithm. For every value of F , the time interval of $T=1200$ was used as a relaxation time to allow the system to reach the steady state, with the time step $\Delta t=0.003$. The averaged velocity defined as

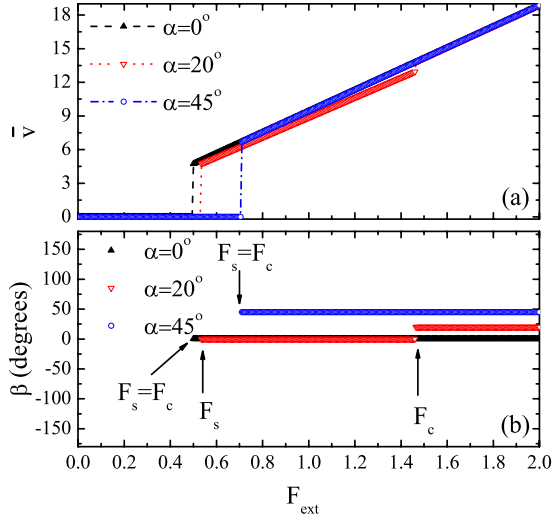


FIG. 1. (Color online) (a) The average atomic velocity \bar{v} as a function of driving force F_{ext} . (b) Intersection angle β as a function of driving force F_{ext} for the case of $\theta=0^\circ$.

$$\bar{v} = \frac{1}{N \times M} \sum_{n=1}^N \sum_{m=1}^M \langle \dot{r}_{n,m} \rangle, \quad (3)$$

where $\langle \rangle$ denotes the time average has been analyzed for different values of the system parameters.

III. NUMERICAL RESULTS

A. Definition of two critical forces F_s and F_c

In Fig. 1(a), the variation in the average atomic velocity of the upper layer with the driving force F_{ext} for $\theta=0^\circ$, $f = \frac{\sqrt{2}}{4}$, $K=1$, and different values of the direction of the external driving force $\alpha=0^\circ, 20^\circ, 45^\circ$ is presented.

As we can see, there exist a critical depinning force at which the system transfers from locked to a sliding state. We define the static friction force F_s as the external driving force at which the average atomic velocity reaches nonzero value [35]. F_s depends on the direction of the external driving force, what is in a good agreement with some results obtained in the studies of superconductors [22].

Variation in the intersection angle β (angle between the x axis and the average atomic velocity or the velocity of the center of mass) with the magnitude of the external driving force is presented in Fig. 1(b). Position of angles α and β is clearly shown in Fig. 2.

The value of the external driving force strongly influences the angles β or the direction in which particles will move. If $F_{\text{ext}} < F_s$, the average velocity of particles is zero. In the region where $F_s < F_{\text{ext}} < F_c$, β is a constant, meanwhile $\beta \neq \alpha$. In this case, the atoms of the upper layer depin from the substrate and start to move in the direction that is different from that of the external driving force.

However, if $F_{\text{ext}} > F_c$, β becomes equal to α . We could then define another critical force F_c as a kinetic friction force at which α changes from $\alpha \neq \beta$ to $\alpha = \beta$ [see Fig. 1(b)]. Therefore, we may conclude that when $F_{\text{ext}} > F_c$ the upper

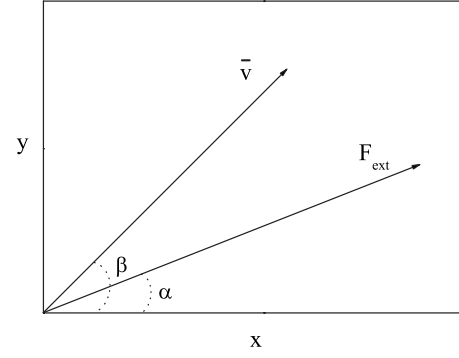


FIG. 2. Definitions of α and β . α is the intersection angle between the direction of the external driving force and the x axis, β is the intersection angle between the direction of the average velocity of atoms and the x axis.

begins to slide exactly in the direction of the external driving force. It is important to note that F_c depends on the system parameter α , i.e., it depends on the direction of the external driving force.

In Fig. 3 the same variation in \bar{v} with F_{ext} as in Fig. 1 but for $\theta=20^\circ$ is presented. Comparing the results in Figs. 1 and 3, we can see that F_s and F_c are strongly dependent on the misfit angle θ .

For the symmetrical case of $\theta=0^\circ$ and $b/a=1$ (see Fig. 1), the switching events can be explained analytically in the following section. In Fig. 3 $\theta=20^\circ$ which is asymmetric case, the switching events are much more complex than those in Fig. 1. When each atom of the system is driven by external driving force, each atom will be forced by three kind of forces. First is the external driving force. Second is the force from the substrate of the lower layer, but the force of each atom is different since $\theta \neq 0^\circ$. In Fig. 1, the second force is same to each atom. The third force is the interaction forces from neighbors in upper layer which is also different for each atom since the distance between two neighbors is usually not same for the case of $\theta \neq 0^\circ$. But the third force to each atom

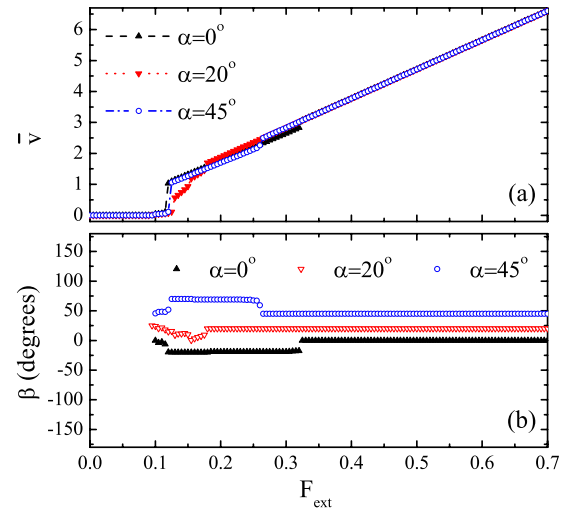


FIG. 3. (Color online) (a) The average atomic velocity \bar{v} as a function of driving force F_{ext} . (b) Intersection angle β as a function of driving force F_{ext} for the case of $\theta=20^\circ$.

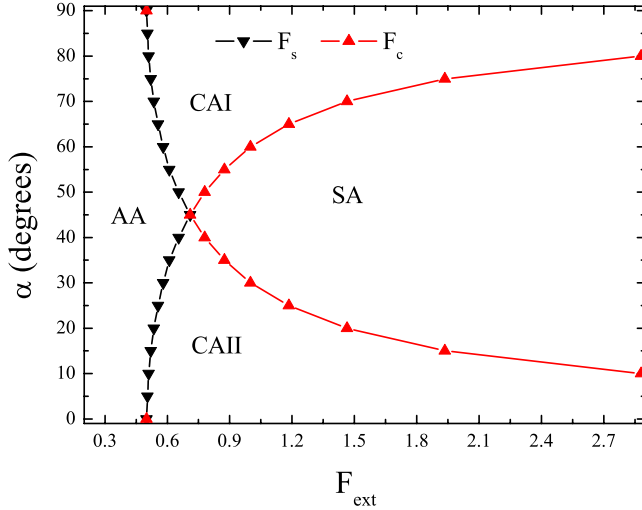


FIG. 4. (Color online) Dependence of the F_s and F_c on the magnitude and the direction of the external driving force where $f = \frac{\sqrt{2}}{4}$, $K=1$, and $\theta=0^\circ$. In the region AA the velocity is zero, in the region CAI $\beta=90^\circ$, in the region CAII $\beta=0^\circ$, in the region SA $\beta = \alpha$. Analytical results are presented by the solid line. The numerical results for F_s , are presented by the inverted triangles, while those for F_c by the regular triangles.

in Fig. 1 is also same. The moving direction of the system is determined by the direction of the sum of this three forces which depend on the external driving force, θ , α , winding number b/a , stiffness of the upper layer K , particle number (or system size) and the substrate potential of the lower layer. Therefore it is too complex to give the analytical result. Usually as the external driving force increases the direction of the sum of the three forces varies, so we can observe the switching events as in Fig. 3.

B. Dependence of F_s and F_c on the external driving force

When $\theta=0^\circ$, the system is equivalent to the commensurate case [35]. In order to understand how both F_s and F_c depend on the system parameters, their variations with the magnitude and the direction of the external driving force ($|F_{\text{ext}}|, \alpha$) are given in Fig. 4. As we can see, the parameter space can be divided into three different regions:

(i) *Region AA (arbitrary angle)* where $F_{\text{ext}} < F_s$ and the average atomic velocity $\bar{v}=0$.

(ii) *Region CA (constant angle)* where $F_s < F_{\text{ext}} < F_c$ and β is a constant while $\beta \neq \alpha$.

(iii) *Region SA (same angle)* where $F_{\text{ext}} > F_c$ and $\beta = \alpha$.

Similar diagram has been obtained in some studies of superconductors [13].

In the region AA ($\bar{v}=0$), the mass center of the upper layer are motionless. In the region CA, \bar{v} has the nonzero value, however the atoms move in the direction different from the direction of the external driving force. According to the direction of the average velocity of the upper layer, region CA can be divided into two different parts CAI and CAII. In the region CAI, $\beta=90^\circ$, and the atoms move in the direction of the y axis, meanwhile in the region CAII $\beta = 0^\circ$, the atoms move in the direction of the x axis. This

result is similar to that observed in previous works on driven vortices in a periodic potential [43,44]. In the region SA, $\beta = \alpha$, the atoms move in the direction of the external driving force.

When $\alpha=45^\circ$, it was found that the static friction force F_s reaches its maximum while F_c reaches its minimum value. At this point, the CA region disappears, and $F_c=F_s$. The atoms of the upper layer are either motionless or move in the direction of the external driving force.

In order to explain the numerical results in Fig. 4 and to understand further the properties of the two critical depinning forces F_s and F_c , in Eq. (2), summation over all $N \times M$ atoms in the system when the system is pinned has been performed: $\sum_{n,m}^{N,M} \frac{\partial(V_{\text{sub}})}{\partial \mathbf{r}_{n,m}} = (N \times M) \mathbf{F}_{\text{ext}}$. For large K , the atoms are nearly equally separated, namely, $x_{n,m} = na + \Delta_x$, $y_{n,m} = ma + \Delta_y$, where $\Delta_x < a$ and $\Delta_y < a$ are uniform shifts for all atoms. When $\theta \neq 0^\circ$, for the most values of system parameters, the sum will be equal to zero if N and M are large enough. In that case, there is no possible stable solution for $F_{\text{ext}} > 0$ and the static friction force will vanish, and therefore, superlubricity may take place, as it was observed in some experiments [37,38]. However, in the case when $\theta = 0^\circ$, the sum will not vanish and static friction force will be different from zero. The external driving force acting on each atom is $(F_{\text{ext}} \cos \alpha, F_{\text{ext}} \sin \alpha)$, while the force from the substrate is $[\sqrt{2}f \sin 2\sqrt{2}\pi(n + \Delta_x), \sqrt{2}f \sin 2\sqrt{2}\pi(m + \Delta_y)]$. The maximum force from the substrate acting on each atom in the x and y directions is $\sqrt{2}f$. If the upper layer is motionless, the conditions $F_{\text{ext}} \cos \alpha = \sqrt{2}f \sin 2\sqrt{2}\pi(n + \Delta_x)$ and $F_{\text{ext}} \sin \alpha = \sqrt{2}f \sin 2\sqrt{2}\pi(m + \Delta_y)$ are satisfied, where $\sin 2\sqrt{2}\pi(n + \Delta_x) \leq 1$ and $\sin 2\sqrt{2}\pi(m + \Delta_y) \leq 1$. Δ_x and Δ_y can be determined from these equations.

As the external driving force increases until $F_{\text{ext}} \cos \alpha \geq \sqrt{2}f$, while $F_{\text{ext}} \sin \alpha < \sqrt{2}f$, in the region $0^\circ \leq \alpha < 45^\circ$, the component of the external driving force in the x direction is larger than that of the depinning force, while its component in the y direction is smaller, and atoms will move in the x direction. When $F_{\text{ext}} \cos \alpha = \sqrt{2}f$, we define critical depinning force F_s as the value of F_{ext} at which the upper layer starts to move in the x direction. Therefore, we obtain $F_s = \frac{\sqrt{2}f}{\cos \alpha}$. As the external driving force continues to increase until $F_{\text{ext}} \sin \alpha \geq \sqrt{2}f$, the external driving force in the y directions will also become larger than its corresponding depinning force and the atoms will start to move in the direction of the external driving force. At this point, when $F_{\text{ext}} \sin \alpha = \sqrt{2}f$, we define another critical force F_c where $F_c = \frac{\sqrt{2}f}{\sin \alpha}$.

Since the system is symmetric around $\alpha=45^\circ$, in the region $45^\circ \leq \alpha < 90^\circ$, the analytical results can be obtained in a similar way. Therefore, the results for F_s and F_c can be given as follows:

$$F_s = \frac{\sqrt{2}f}{\cos \alpha}, \quad (4)$$

$$F_c = \frac{\sqrt{2}f}{\sin \alpha} \quad (5)$$

in the region $0^\circ < \alpha \leq 45^\circ$ and

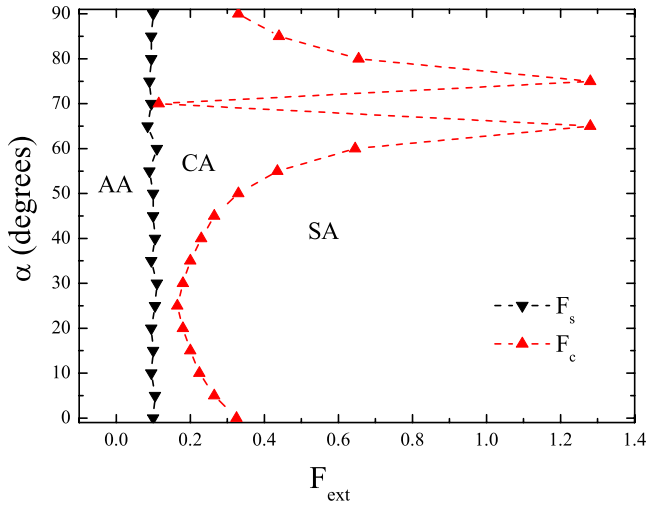


FIG. 5. (Color online) Dependence of the F_s and F_c on the magnitude and the direction of the external driving force where $f = \frac{\sqrt{2}}{4}$, $K=1$, and $\theta=20^\circ$. In the region AA, the velocity of the center of mass is zero, in the region SA $\beta=\alpha$.

$$F_s = \frac{\sqrt{2}f}{\sin \alpha}, \tag{6}$$

$$F_c = \frac{\sqrt{2}f}{\cos \alpha} \tag{7}$$

in the region $45^\circ \leq \alpha < 90^\circ$

The analytical results in Eqs. (4)–(7) are presented in Fig. 4 by solid line, while the numerical results for F_s and F_c from Eq. (2) are presented in the same figure by black inverted triangle and red triangle, respectively. As we can see there is an excellent agreement between results. For the case $\theta \neq 0^\circ$, the results are similar.

A special case for $\theta=20^\circ$ is shown in Fig. 5. There are also three regions of AA, CA, and SA that correspond to $F_s < F_{\text{ext}}$, $F_s < F_{\text{ext}} < F_c$, and $F_c < F_{\text{ext}}$, respectively. In Fig. 5, we note that the curve of F_c vs α for $\theta=20^\circ$ have peaks at the points of approximately $\alpha=65^\circ$ and $\alpha=75^\circ$. We find that both critical forces of F_s and F_c depend on the misfit angle θ . F_s is much smaller in the case of $\theta \neq 0^\circ$ than that of $\theta=0^\circ$. It is also noted that it is too complex for the general case of $\theta \neq 0$ and $\alpha \neq 0$. In the following we will note that the dependence of F_s on the θ is fractal structures. Therefore, the variations of F_s and F_c versus θ and α are very complex. In this paper we will mainly focus on the simple cases of $\theta=0$, $\alpha \neq 0$ or $\theta \neq 0$, $\alpha=0$.

In the following section we will study the dependence of F_s and F_c on the misfit angle θ in detail.

C. Dependence of F_s and F_c on the misfit angle θ

Variations of the F_s and F_c with the magnitude of the external driving force $|F_{\text{ext}}|$ and the misfit angle θ are presented in Fig. 6. As in Fig. 4, we can distinguish three regions AA, CA, and SA for $F_{\text{ext}} < F_s$, $F_s < F_{\text{ext}} < F_c$, and $F_{\text{ext}} > F_c$, respectively.

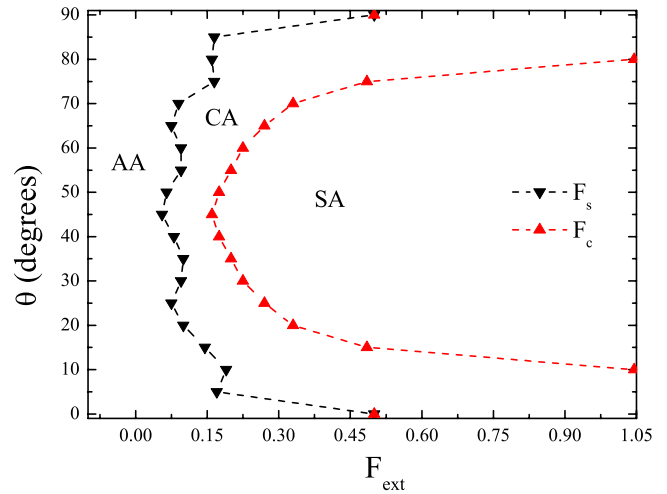


FIG. 6. (Color online) Dependence of the F_s on the misfit angle θ for $f = \frac{\sqrt{2}}{4}$, $K=1$, and $\alpha=0^\circ$.

In the region AA, the velocity of particles is zero, meanwhile in the region CA, it has a finite value, but it is in different direction from that of the external driving force. In the region SA, particles move in the direction of driving force. As we can see in Fig. 6, both critical forces, F_s and F_c , strongly depend on the misfit angle θ . F_s reaches its maximum value when $\theta=0^\circ$ or 90° , while F_c reaches its minimum at $\theta=45^\circ$ and maximum at $\theta=0^\circ$ or 90° . The numerical analysis have been also performed for other values of $\alpha \neq 0^\circ$, and the obtained results are qualitatively similar with the presented one. One of these results, the special case for $\alpha=20^\circ$ is presented in Fig. 7, in which we note that the curve of F_c vs θ for $\alpha=20^\circ$ have peaks at the points of approximately $\theta=65^\circ$ and $\theta=75^\circ$.

In order to better understand the dependence of the F_s on the θ , variation in F_s with θ for two regions of θ , $42.0^\circ < \theta < 48.0^\circ$ and $46.5^\circ < \theta < 47.5^\circ$ is presented in Figs. 8 and 9, respectively. Remarkably, the dependence of F_s and F_c on θ looks like a fractal structure. To verify this conclusion, we

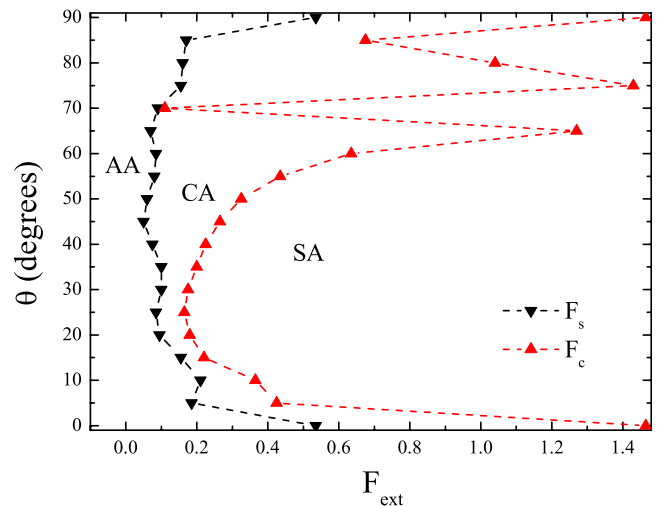


FIG. 7. (Color online) Dependence of the F_s on the misfit angle θ for $f = \frac{\sqrt{2}}{4}$, $K=1$, $\alpha=20^\circ$.

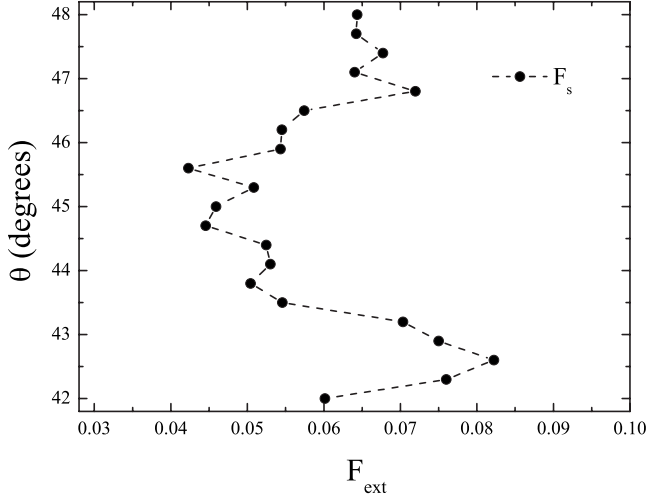


FIG. 8. Dependence of the F_s on the misfit angle θ for $f=\frac{\sqrt{2}}{4}$, $K=1$, $\alpha=0^\circ$ in the region of $42.0^\circ < \theta < 48.0^\circ$.

have studied the dependence of F_s on the θ on much smaller scale within our degree of the computer accuracy. We found the fractal structure in the dependence of F_s on the θ . The corresponding dimension of the fractal structure is obtained by the equation of $d=1-\log_{10} \frac{L}{L_0}$, where $L=\sum_i \sqrt{\theta_i^2 + F_{si}^2}$, $l=\sum_i \sqrt{\theta_i^2 + F_{si}^2}/N$, $L_0=L$ when dimension $d=1$. We use $\delta f=0.0001$ and $F_{si}=F_0+i\delta f$, $i=1, \dots, 50$. The fractal dimension as a function of θ is shown in Fig. 10. It indicates that the fractal dimension is not a constant, but it is a function of the misfit angle θ .

D. Dependence of F_s and F_c on interaction strength between atoms K

The dependence of F_s and F_c on the strength of the interatomic interaction K for four different values of θ and α is shown in Fig. 11. For $\theta=0^\circ$ and $\alpha=0^\circ$ in Fig. 11(a), $F_s=F_c$ and they are independent of the K . This result is equivalent to the result obtained in one-dimensional case [35]. In this

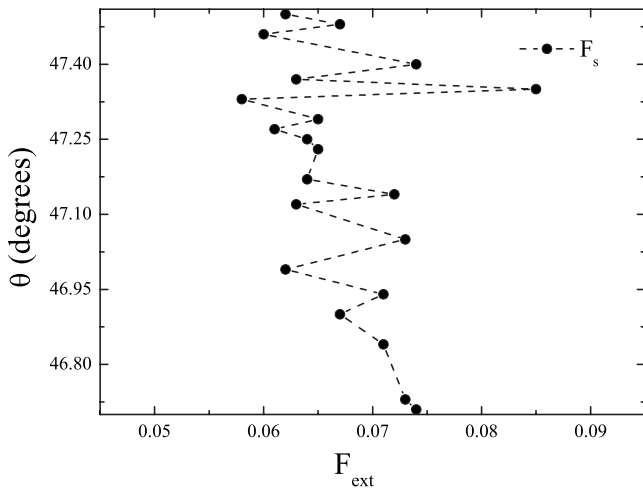


FIG. 9. Dependence of the F_s on the misfit angle θ for $f=\frac{\sqrt{2}}{4}$, $K=1$, $\alpha=0^\circ$ in the region of $46.7^\circ < \theta < 47.5^\circ$.

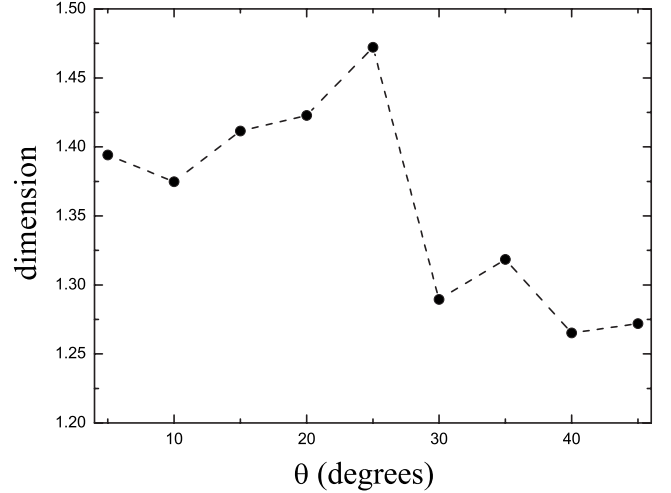


FIG. 10. Dependence of the fractal dimension on the misfit angle θ , where $f=\frac{\sqrt{2}}{4}$, $K=1$, $\alpha=0^\circ$.

case, there are only two regions: AA and SA. In the region AA, the particles are motionless. In region SA, they move in the direction of external driving force. The analytical form for F_s in this case can be given as $F_s=\sqrt{2}f$ what is in good agreements with the numerical results. In Fig. 11(b), the results for $\theta=0^\circ$ and $\alpha=20^\circ$ are presented. In this case, F_s and F_c are different but still independent of the parameter K . There are three regions of AA, CA, and SA that correspond to the $F_{\text{ext}} < F_s$, $F_s < F_{\text{ext}} < F_c$, and $F_{\text{ext}} > F_c$ respectively. The analytical results for both F_s and F_c can be given as: $F_s = \frac{\sqrt{2}f}{\cos 20^\circ}$, and $F_c = \frac{\sqrt{2}f}{\sin 20^\circ}$, what is in good agreements with the numerical ones. After performing simulations for other values of α at $\theta=0^\circ$, we came to the conclusion that two critical depinning forces F_s and F_c are independent of the parameter K . Their analytical form can be obtained from Eqs. (4)–(7).

However, if $\theta \neq 0^\circ$, the results are quite different, as we can see in Figs. 11(c) and 11(d) for $\theta=20^\circ$, $\alpha=0^\circ$ and $\theta=20^\circ$, $\alpha=20^\circ$, respectively. As the parameter K increases, F_s decreases until K reaches a critical value $K_{c1} \approx 2$. When $K > K_{c1}$, F_s remains approximately independent of the K . It becomes as small as about the order of 10^{-2} , in which case superlubricity may take a place. Meanwhile F_c first decreases with the increase in K until $K=K_{c2} \approx 1$, and then it increases as K continues to increase.

E. Dependence of F_s and F_c on the magnitude of the adhesive force from substrate f

In Fig. 12, the numerical results for F_s and F_c as a functions of the adhesive force from substrate are presented for four different cases: (a) $\theta=0^\circ$, $\alpha=0^\circ$, (b) $\theta=0^\circ$, $\alpha=20^\circ$, (c) $\theta=20^\circ$, $\alpha=0^\circ$, and (d) $\theta=20^\circ$, $\alpha=20^\circ$. As we can see, in Fig. 12(a), there are only two regions: AA and SA. The analytical result for F_s has the form $F_s=\sqrt{2}f$, and it is in a good agreement with the numerical one. For other cases shown in Figs. 12(b)–12(d), we can see that there are three regions AA, CA, and SA that correspond to $F_{\text{ext}} < F_s$, $F_s < F_{\text{ext}} < F_c$, $F_{\text{ext}} > F_c$, respectively. As f increases both F_s and F_c increase. For $\theta=0^\circ$ and $\alpha=20^\circ$, the analytical results for F_s and F_c are given

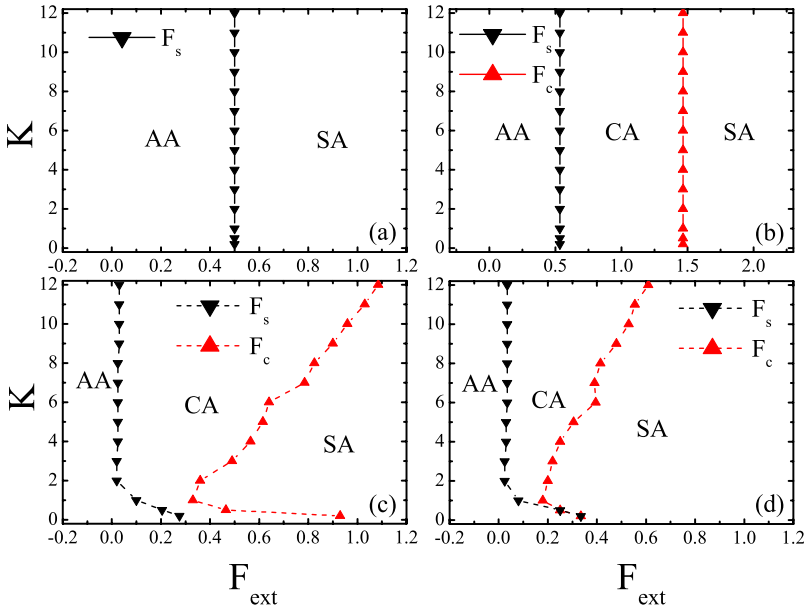


FIG. 11. (Color online) Dependence of the F_s and F_c on the magnitude of the external driving force F_{ext} and the strength of the interatomic interaction between atoms of the upper layer K , where $f = \frac{\sqrt{2}}{4}$. (a) $\theta=0^\circ$, $\alpha=0^\circ$, the analytical result is expressed by solid line, the numerical results are expressed by triangles, (b) $\theta=0^\circ$, $\alpha=20^\circ$, (c) $\theta=20^\circ$, $\alpha=0^\circ$, the analytical result is expressed by solid line, the numerical results are expressed by triangles, (d) $\theta=20^\circ$, $\alpha=20^\circ$.

as follows: $F_s = \frac{\sqrt{2}f}{\cos 20^\circ}$, and $F_c = \frac{\sqrt{2}f}{\sin 20^\circ}$, which are in a good agreement with the numerical ones, as can be seen in Fig. 12(b). We have to note that when $\theta \neq 0^\circ$, the static friction force is much smaller. As f goes to zero the static friction force also goes to zero, as it is shown in Figs. 11(c) and 11(d).

In Fig. 13, the numerical results for F_s and F_c as a functions of the adhesive force from substrate are also presented in which we take parameter $K=1$ which is different from Fig. 12 ($K=12$). We note the similar results between two. However, for smaller K in Fig. 13 when $\theta=20^\circ$ and $\alpha=20^\circ$ there are only two regions of AA and SA if external driving force is large enough. In other word, For smaller K when external driving force large enough $F_s = F_c$.

According to the above results, we may conclude that in order to obtain superlubricity, materials with smaller f and larger K have to be used. Though this result is similar with

that in 1D case, this suggest that in a more real 2D case, the same results is found. Meanwhile the misfit angle has to be chosen in a suitable way in order to obtain smaller friction force.

IV. CONCLUSION

The locked-to-sliding phase transition for certain materials with square lattice symmetry has been studied in the 2DFK model. With the increase in external driving force, at some critical value the system transfers from the lock to the sliding state where the particles move in the direction different from that of driving force. With the further increase in external force, at some critical value, the motion of particles becomes aligned with the direction of driving force. The values of external driving force at these two critical points have been defined as two different friction forces. They both de-

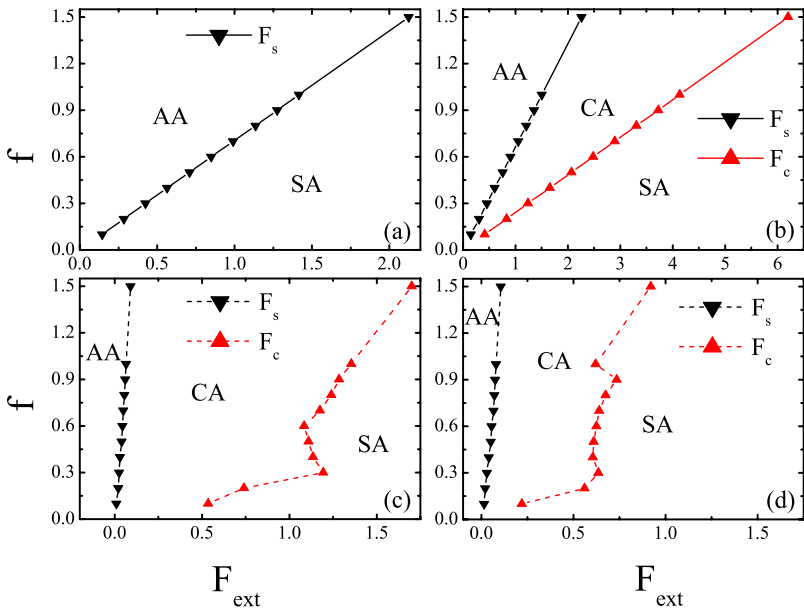


FIG. 12. (Color online) Dependence of the F_s and F_c on the magnitude of the external driving force F_{ext} and the strength of substrate potential from lower layer f for $K=12$, and different values of θ and α : (a) $\theta=0^\circ$, $\alpha=0^\circ$, (b) $\theta=0^\circ$, $\alpha=20^\circ$, (c) $\theta=20^\circ$, $\alpha=0^\circ$, and (d) $\theta=20^\circ$, $\alpha=20^\circ$.

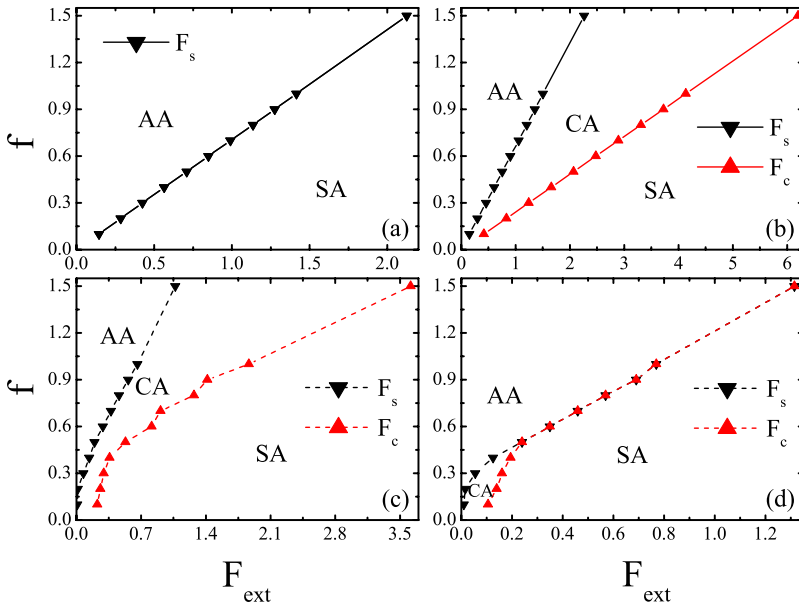


FIG. 13. (Color online) Dependence of the F_s and F_c on the magnitude of the external driving force F_{ext} and the strength of substrate potential from lower layer f for $K=1$, and different values of θ and α : (a) $\theta=0^\circ$, $\alpha=0^\circ$, (b) $\theta=0^\circ$, $\alpha=20^\circ$, (c) $\theta=20^\circ$, $\alpha=0^\circ$, and (d) $\theta=20^\circ$, $\alpha=20^\circ$.

pend on the direction and the value of external driving force, the magnitude of adhesive force and the interaction strength between two atoms in the upper layer and especially on the misfit angle θ . For some values of misfit angle, the friction force is very small what is in a good agreement with some recent experimental results [37,38]. The phase diagram of the system with three different regions (AA, CA, and SA) that correspond to different dynamical behavior has been obtained. For zero misfit angle, the analytical expressions for two critical forces F_s and F_c are obtained which are in agreement with the numerical ones. If the misfit angle $\theta \neq 0^\circ$, it was found that dependence of static friction force F_s on the misfit angle θ was in fractal structure, where dimensions of the fractals have been given.

Since the system is driven by an external driving force, the damping term play a crucial role to let the system reach steady state or equilibrium in a short period. Otherwise, the system cannot reach the equilibrium state which is not the real case. Therefore, in our simulation of this paper, damping term play an important role. However, it is different from the overdamped case. For overdamped case the system can reach steady state in a shorter period than that in the underdamped case. The larger the damping term, the shorter period needed to reach steady state for the system. Moreover, in the overdamped case the average particle velocity or other system variables at the critical point are continuous or nearly con-

tinuous, but in the underdamped case they are discontinuous. The inertia term of the particle for the overdamped case can be neglected, however, in the underdamped system the inertia term cannot be neglected.

In order to obtain superlubricity between two layers, we will choose the materials with the larger interatomic interaction strength of the upper layer, and the smaller magnitude of adhesive force of the lower layer. This conclusion is similar with that found in 1D case. Meanwhile, the suitable misfit angle had to be chosen in order to obtain smaller friction force.

For the smaller size the time for simulation is shorter, so we get the results for the relatively small system of 12×12 particles. The results actually depends on how many particles of the system, but the results are qualitatively same. How the results depends on the system size is also a problem which will be solved in the future.

ACKNOWLEDGMENTS

The work was in part supported by the 100 Person Project of the Chinese Academy of Sciences, the China National Natural Science Foundation with Grants No. 10775157 and No. 10875098, and the Natural Science Foundation of Northwest Normal University (Grant No. NWNNU-KJCXGC-03-48). We thank Professor Alexander Savin for helpful discussions and suggestions.

[1] G. Blatter, M. V. Feigel'man, V. B. Geshkenbein, A. I. Larkin, and V. M. Vinokur, *Rev. Mod. Phys.* **66**, 1125 (1994).
 [2] A. C. Marley, M. J. Higgins, and S. Bhattacharya, *Phys. Rev. Lett.* **74**, 3029 (1995).
 [3] G. Grüner, *Rev. Mod. Phys.* **60**, 1129 (1988).
 [4] C. Reichhardt and C. J. Olson Reichhardt, *Phys. Rev. Lett.* **92**, 108301 (2004).
 [5] C. Reichhardt, C. J. Olson, N. Gronbech-Jensen, and F. Nori, *Phys. Rev. Lett.* **86**, 4354 (2001).
 [6] A. A. Middleton and N. S. Wingreen, *Phys. Rev. Lett.* **71**, 3198 (1993).
 [7] C. Reichhardt and C. J. Olson Reichhardt, *Phys. Rev. Lett.* **90**, 046802 (2003).
 [8] R. Seshadri and R. M. Westervelt, *Phys. Rev. B* **46**, 5150 (1992).
 [9] B. N. J. Persson, *Sliding Friction: Physical Principles and*

- Applications* (Springer-Verlag, Berlin, 1998); *Surf. Sci. Rep.* **33**, 83 (1999).
- [10] O. M. Braun, I. Barel, and M. Urbakh, *Phys. Rev. Lett.* **103**, 194301 (2009).
- [11] D. Cule and T. Hwa, *Phys. Rev. Lett.* **77**, 278 (1996); *Phys. Rev. B* **57**, 8235 (1998).
- [12] A. I. Larkin and Yu. N. Ovchinnikov, *Zh. Eksp. Teor. Fiz.* **65**, 1704 (1973) [*Sov. Phys. JETP* **38**, 854 (1974)].
- [13] H. J. Jensen, A. Brass, and A. J. Berlinsky, *Phys. Rev. Lett.* **60**, 1676 (1988); A. Brass, H. J. Jensen, and A. J. Berlinsky, *Phys. Rev. B* **39**, 102 (1989); H. J. Jensen, Y. Brechet, and A. Brass, *J. Low Temp. Phys.* **74**, 293 (1989).
- [14] U. Yaron *et al.*, *Nature (London)* **376**, 753 (1995).
- [15] F. Pardo *et al.*, *Nature (London)* **396**, 348 (1998).
- [16] G. D'Anna, P. L. Gammel, H. Safar, G. B. Alers, D. J. Bishop, J. Giapintzakis, and D. M. Ginsberg, *Phys. Rev. Lett.* **75**, 3521 (1995); T. Tsuboi, T. Hanaguri, and A. Maeda, *ibid.* **80**, 4550 (1998).
- [17] C. J. Olson, C. Reichhardt, and F. Nori, *Phys. Rev. Lett.* **81**, 3757 (1998).
- [18] C. Reichhardt, C. J. Olson, and F. Nori, *Phys. Rev. Lett.* **78**, 2648 (1997); *Phys. Rev. B* **58**, 6534 (1998).
- [19] C. Reichhardt and N. Gronbech-Jensen, *Phys. Rev. B* **63**, 054510 (2001).
- [20] C. Reichhardt, G. T. Zimányi, and N. Gronbech-Jensen, *Phys. Rev. B* **64**, 014501 (2001).
- [21] C. Reichhardt, G. T. Zimányi, R. T. Scalettar, A. Hoffmann, and I. K. Schuller, *Phys. Rev. B* **64**, 052503 (2001).
- [22] C. Reichhardt, C. J. Olson, and M. B. Hastings, *Phys. Rev. Lett.* **89**, 024101 (2002).
- [23] O. M. Braun, A. R. Bishop, and J. Röder, *Phys. Rev. Lett.* **79**, 3692 (1997); M. Paliy, O. Braun, T. Dauxois, and B. Hu, *Phys. Rev. E* **56**, 4025 (1997); O. M. Braun, B. Hu, A. Filippov, and A. Zeltser, *ibid.* **58**, 1311 (1998); O. M. Braun, H. Zhang, B. Hu, and J. Tekić, *ibid.* **67**, 066602 (2003).
- [24] O. M. Braun and Y. S. Kivshar, *Phys. Rep.* **306**, 1 (1998).
- [25] A. Vanossi and O. M. Braun, *J. Phys.: Condens. Matter* **19**, 305017 (2007).
- [26] Z. G. Shao, L. Yang, H. K. Chan, and B. Hu, *Phys. Rev. E* **79**, 061119 (2009).
- [27] J. Tekić, D. He, and B. Hu, *Phys. Rev. E* **79**, 036604 (2009).
- [28] R. Pushpa, J. Rodriguez-Laguna, and S. N. Santalla, *Phys. Rev. B* **79**, 085409 (2009).
- [29] D. Rodney and L. Proville, *Phys. Rev. B* **78**, 104115 (2008).
- [30] S. P. Fitzgerald and D. Nguyen-Manh, *Phys. Rev. Lett.* **101**, 115504 (2008).
- [31] A. N. Kolmogorov and V. H. Crespi, *Phys. Rev. B* **71**, 235415 (2005).
- [32] O. M. Braun, T. Dauxois, M. V. Paliy, and M. Peyrard, *Phys. Rev. E* **55**, 3598 (1997).
- [33] E. Granato and S. C. Ying, *Phys. Rev. B* **59**, 5154 (1999).
- [34] T. Kawaguchi and H. Matsukawa, *Phys. Rev. B* **61**, R16366 (2000).
- [35] C. L. Wang, W. S. Duan, J. M. Chen, and X. R. Hong, *Appl. Phys. Lett.* **93**, 153116 (2008).
- [36] J. Tekić, O. M. Braun, and B. Hu, *Phys. Rev. E* **71**, 026104 (2005).
- [37] M. Hirano, K. Shinjo, R. Kaneko, and Y. Murata, *Phys. Rev. Lett.* **78**, 1448 (1997).
- [38] M. Dienwiebel, G. S. Verhoeven, N. Pradeep, J. W. M. Frenken, J. A. Heimberg, and H. W. Zandbergen, *Phys. Rev. Lett.* **92**, 126101 (2004).
- [39] B. N. J. Persson, O. Albolu, U. Tartaglino, A. I. Volokitin, and E. Tosatti, *J. Phys.: Condens. Matter* **17**, R01 (2005).
- [40] H. Li, T. Xu, C. Wang, J. Chen, H. Zhou, and H. Liu, *Tribol. Int.* **40**, 132 (2007).
- [41] H. Holscher, U. Schwarz, and R. Wiesendanger, *Surf. Sci.* **375**, 395 (1997).
- [42] P. Steiner, R. Roth, E. Gnecco, A. Baratoff, S. Maier, T. Glatzel, and E. Meyer, *Phys. Rev. B* **79**, 045414 (2009).
- [43] C. Reichhardt and F. Nori, *Phys. Rev. Lett.* **82**, 414 (1999).
- [44] E. Granato and S. C. Ying, *Phys. Rev. Lett.* **85**, 5368 (2000).